Research Article

Ali K. Al-Asadi*, Salih K. Alrebeh and Waleed Kh. Hadi

Experimental investigation of RC beams strengthened with externally bonded BFRP composites

https://doi.org/10.1515/eng-2022-0548
received July 16, 2023; accepted October 30, 2023

Abstract

Objectives – The goal of this article is to examine the behavior of reinforced concrete (RC) rays that strengthen superficially the basalt fiber-reinforced polymer (BFRP) fabrics. We found out that one ray without BFRP and seven rays enveloped within numerous lay-up arrangements. The importance of the study is to improve the flexural capacity of rays, using fiber-reinforced polymer procedure and examine the over-reinforcement technique.

Methods – Interestingly, we have examined under two-point loading, one BFRP fabric sheet flexure.

Results – Loads corresponding to the first crack/delamination and ultimate failure of the beams have been verified. Moreover, we have recognized the types of failure and load contrasted with deflection graphs that have been strategized at outstanding ray locations.

Novelty – Our investigation has unraveled the increased flexural strength of the strengthened RC rays after using coating. Additionally, we have applied pressure to the BFRP fabrics on both sides of the beams. Moreover, we have improved performance with flexural strength, ductility, and failure. Our results are novel and show that the flexural capacity of the wrapped RC rays increases by 46.6%. The ductility increased by 84%, and unfortunately, we had failed the FRB and the concrete had crushed.

Keywords: strengthening basalt fiber-reinforced polymer, reinforcement concrete RC beams, rays, externally bonded, flexural behavior, ductility

*** Corresponding author: Ali K. Al-Asadi,** College of Engineering University of Thi-Qar, Thi-Qar, Iraq, e-mail: Alazharco.2005@utq.edu.iq
Salih K. Alrebeh: College of Engineering University of Thi-Qar, Thi-Qar, Iraq
Waleed Kh. Hadi: College of Engineering, Mazaya University College, Thi-Qar, Iraq

1 Introduction

Production of novel fiber-reinforced polymer (FRP) is gaining increased attention worldwide [1–7]. Basalt fiber-reinforced polymer (BFRP) is a novel kind of inorganic fiber that is robust and armored. As the name suggests, basalt fiber is composed of pure natural basalt, which is less expensive than carbon fibers. Basalt fiber is unique because of its high strength, good durability, remarkable fire resistance and electrical insulation, and resistance to acid, alkali, and chemical corrosion [8–10]. A considerable number of research works have investigated fiber. Nevertheless, some of it has been performed on the consolidation of reinforced concrete (RC) beams/girders using lightly joined BFRP laminates/sheets.

Other researchers have examined the mechanical and basalt fibers' stability and concluded that they display durable stability weathering. Moreover, it showed high-temperature criteria as associated with glass or carbon fibers [11]. Likewise, basalt fibers originate from volcanic rock [12]. Fabric, along with other forms, might be used as clearly combined combinations for consolidation and recovery of various structural components. The superficially fused FRP combinations in solidification beams in flexure reach the limit of their presence with the fibers involved in the longitudinal route. According to Sim et al. and Lihua et al., BFRP is noticeably devoted when used as a flexural hardening agent for RC beams. The modifications fortified RC rays with variable numbers of layers positioned to one direction BFRP sheets and learned that a higher number of layers of BFRP augmented beams with final measurements. Nevertheless, these experiments found that if sparse distance is selected, failure by interfacial deboning can arise, which is unwanted.

Fiore et al. [13] have indicated that based on the mechanical properties of BFRP, the load capacity of the structural element has improved. Additionally, owing to the high compressive properties of BFRP, RC components have a greater strength capability based on the experimental study completed. According to Pawłowski and Szumigała [14], the RC

beam increased by BFRP acted as linearly as possible for failure. According to Shen et al. [15], the central assumptions have been reported that the RC box beam repaired with BFRP reduces the progress of concrete flaws. Moreover, the toughness and natural frequency of the renovated beam were increased by 16.6 and 8.0%, respectively, in comparison to the naked ray.

According to the experimental work of Qin et al. [16], the application of a two-point load has twisted severely pre-cracked RC beams braced with BFRP sheets to their intact state.

According to the experimental studies conducted by other researchers [17,18], pre-cracks in the concrete had no effect on the RC ray enhanced by BFRP. The cost of structural element remediation is nearly equal to the cost of permutation, so the process would become cost-effective. Ma et al. [19] reported that the flexural capacity of RC specimens strengthened with BFRP sheets can be significantly improved, and the BFRP sheets can limit the crack propagation of concrete structures and improve their ductility [20].

Several researchers have documented the use of BFRP sheets in the seismic solidification of building and bridge structures. Lu et al. [21–23] conducted a training on the seismic earthquake-damaged concrete edge joints covered with BFRP. Only a few studies on the use of BFRPs in concrete beams for flexural strengthening are available [24]. As a consequence, analysis of the use of BFRP materials for flexural RC beams is considered necessary. As a matter of fact, this article offers a presentation test of RC beams reinforced with basalt fabrics as a composite.

2 Experimental program

The current study uses a trial to extrapolate the structural behavior of RC beams by wrapping those beams in BFRP fabric. Different BFRP wrapping patterns were used to achieve the aim of this work. Eight RC beams were prepared and tested. One of these beams was used as a reference beam (without using BFRP fabric). The strategy for testing the RC beams was by applying the two-point loading. All the beams have the same dimensions. The material qualifications are presented in the following sub-sections.

2.1 Material properties

2.1.1 Ordinary Portland cement

A Portland cement CEM I 42.5R based on Turkish qualifications TS EN 197 [25] was used in this work to manufacture self-compacting concrete (SCC) for comparison purposes.

2.1.2 Fly ash (FA)

Class F. FA was utilized for fixing the RC specimens, as shown in Figure 1. Furthermore, FA is a very beneficial material, which has a spherical microstructure and affords high flow ability. It was delivered by warm air control Ceyhan Sugözü Turkish herb [26].

2.1.3 Aggregates

The local coarse aggregate was used with a nominal size of 10 mm, while the river sand and fine crushed stone were used as the fine aggregate with a maximum size and specific gravity of 2.6. Figure 2 shows the aggregate used in the mix design of all samples, while Figure 3 shows the volumetric pitches of the rough and fine collections.

2.1.4 Superplasticizer

Figures 3 and 4 show that sulfonated naphthalene formaldehyde has a declining additive specific gravity of 19. The superplasticizer was transformed across the mixing process in order to improve the assortment's workability. Superplasticizer was purchased from a neighborhood provider; all information is shown in Table 1.

2.1.5 BFRP fabrics and resin

In this study, the RC beams were strengthened using unidirectional BFRP fabric. This type of fabric was chosen because of its fire resistance, availability, smooth consistency, resilience, low

Figure 1: FA picture that was employed in the fixing RC.

Figure 2: Aggregates used in the mix design. (a) Coarse aggregate. (b) Fine aggregate. (C) Fine crushed stone.

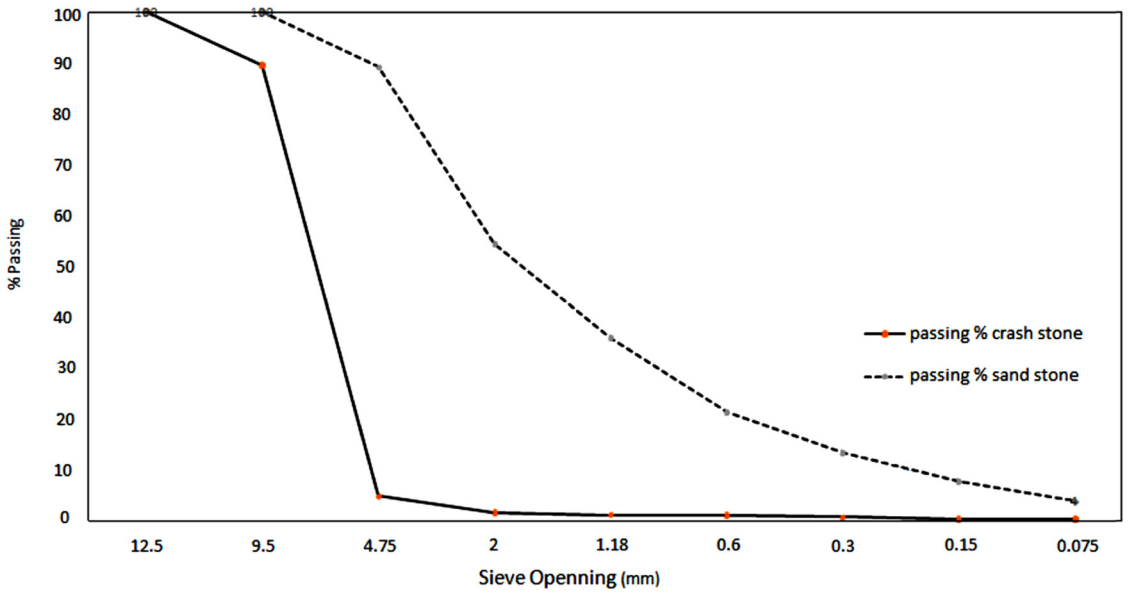

Figure 3: Gradients of volume for rough and small smash aggregate.

price, and high tensile as compared to fabric. The mechanical features of the fabric are displayed in Table 2. More details of the epoxy used, Master Brace 4500 epoxy resin, were linked to the BFRP fabric on the exterior concrete side. According to the company, the epoxy resin had a compressive strength greater than 60 MPa, a bending strength greater than 50 MPa, and a bond strength greater than 3 MPa. The necessary amount of epoxy (A + B) is added in a 3:1 ratio. Figure 5 displays epoxy resin that connects to BFRP sheets. The procedural text determined upon the presentation of the bonding agent to the ray

Figure 4: Superplasticizer used in our study.

Table 1: Characteristics of superplasticizer

Belongings	Superplasticizer
Term	Viscocrete 30
Color	Dark brown
State	Liquid
Specific gravity (kg/l)	1.07
Chemical composition	Modified polycarboxylic-type polymer
Amount	1–2% (% binder content)

Table 2: Dimensions and properties of basalt fiber fabric

Tensile strength (MPa)	Tensile modulus of elasticity (GPa)	Elongation (%)	Thickness (mm)	Area weight (g/m^2)
2,100	105	2.6	0.3	300

examination samples. The mechanical characteristics of the used epoxy resin have been described in detail by an independent group of scientists [27].

3 Specimen preparation

The theoretical capacity of beams depends on external reinforcement. The dimensions and system of steel reinforcement for all specimens were similar. The dimensions of each specimen were 100 mm × 150 mm × 1,000 mm. In addition to the 8 mm stirrups that measure 75 mm from center to center, the specimens' system of reinforcing bars consists of four longitudinal steel bars, two of which have a diameter of 10 mm at the tension zone, and the other two bars have a diameter of 8 mm at the compression zone. For 8 and 10 mm steel bars, respectively, the produce asset of reinforcement bars is 550 and 485 MPa, and the ultimate strength is 640 and 595 MPa. The concrete cover for all beams was 25 mm. Figure 6 shows the beam dimensions and reinforcement facts.

4 Mixture casting and curing condition

4.1 Mix design

The preparation of SCC has differed from that of conventional concrete due to the difference in placing and filling manner. SCC was chosen for use in experimental investigations since it included FA. SCC improves concrete-to-concrete interaction and eliminates the need for a compression process. In addition, FA is a very advantageous material, has a sphere-shaped microstructure, and offers excellent fluidity. Supplemental materials were also used to make SCC with the required fresh properties, such as superplasticizers and crushed stones. Table 3 shows the mixing ratio of SCC [28].

4.2 Casting and curing condition

Table 3 shows the weighted quantities of required materials needed for the two batches. First, the fine and coarse aggregates were mixed in dry conditions for 2 min. Then, the binder materials containing cement, FA, and crushed sand were added with half the amount of the water and mixed for 1 min. Finally, the remaining water and superplasticizers were pre-mixed and poured into the mixture with another 2 min of mixing to consist of the mixture contents. After the mixing procedure was complete, the concrete was poured into the molds immediately without compaction. The steps of casting and curing are illustrated in Figure 7. The beams are covered and left for 24 h in the casting room. After completion of concrete casting, all tested beams were cured in a water tank at laboratory temperature for 28 days. Before starting the test procedure, the compressive strength test was made for six cylinders (100 mm × 200 mm).

Figure 5: Epoxy resin used for bonding and BFRP sheets.

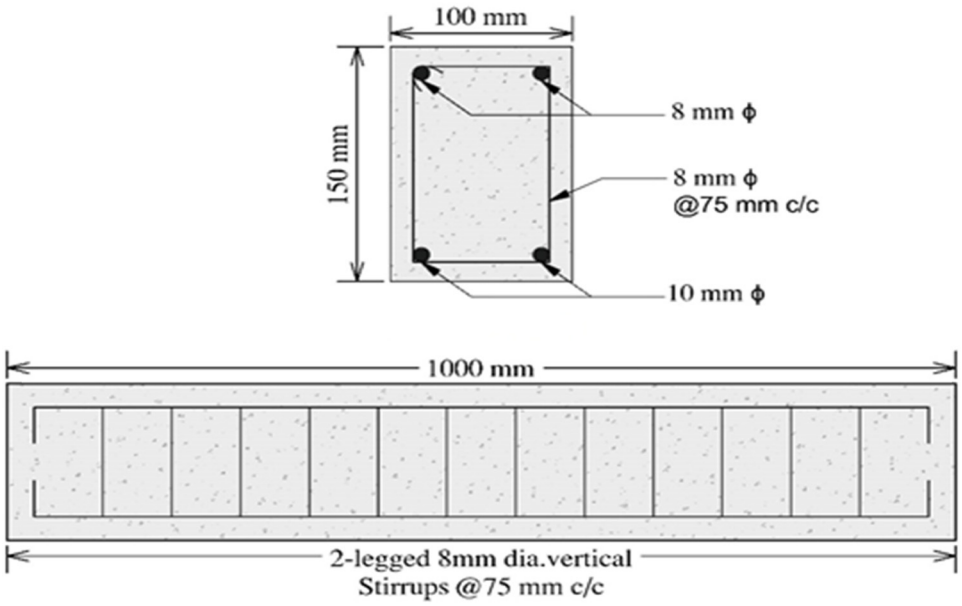

Figure 6: Dimensions and reinforcement of RC beam.

5 Surface and wrapping preparation

(a) Preparing the concrete surface,
(b) Preparing BFRP, and
(c) Impregnating and applying the BFRP fabric.

As shown in Figure 8, a concrete mincer with a rotating disk was served to form the concrete surface by expelling a laitance layer and concrete crumpling. Beams' lower sides were rotated with a radius of about 0.5 in. [29] to evade the concentration stress, which led to premature rupture of the BFRP sheets in accordance with ACI 440.2R [30].

6 Wrapping of BFRP fabrics

Wet lay-up technique (ACI 440 2008) was used to construct the BFRP laminate system [31,34,35].

To complete the implementation of the research, the test was performed for eight RCs.

The first BFRP free beam sheet was categorized as B1 and presented in Figure 9.

The second beam, known as B2 (Figure 10), had a single layer of BFRP textiles covering it entirely at the lowest point and at a height of 25 mm on both sides from the bottom.

The third beam, designated as B3, was entirely covered with BFRP fabrics at the lowest part and 75 mm high at both edges from the lowest part in one layer. It is shown in Figure 11.

The fourth beam, designated as B4, was coated completely with BFRP fabrics at the bottom portion and 105 mm high at both sides from the bottom in one layer (Figure 12).

The fifth beam, designated as B5, was covered completely with BFRP sheets just at the lowest part in one layer (Figure 13).

The sixth beam, designated as B5, was wrapped BFRP with three stirrups in the flexural zone; the distance between stirrups is 10 cm (Figure 14).

Table 3: Mixing ratio and concrete properties [28]

Cement (kg/m^3)	FA (kg/m^3)	Coarse aggregate (kg/m^3)	River sand (kg/m^3)	Crushed sand (kg/m^3)	Water (kg/m^3)	Superplasticizer (kg/m^3)	f'_c (MPa)	Density (kg/m^3)
275	285	710	651	217	188.1	2.77	41.0	2338.27

Figure 7: Steps casting and curing.

The seventh beam, designated as B7, was covered completely with BFRP fabrics at the lowest portion, plus stirrups in the flexural zone in one layer (Figure 15).

The eighth beam, designated as B7, was covered completely with BFRP sheets except for the upper surface part in one layer (Figure 16).

All samples were kept for 1 week air curing at a temperature of 27 ± 2°C before starting the test.

7 Flexural test setup and instrumentation

RC beams, both with and without BFRP fabrics, every single sample, were investigated under a static two-point load. For the assessment process, an INSTRON testing machine, as demonstrated in Figure 8, was utilized, which includes a hydraulic with a load size of 250 kN with a

Figure 8: Configuration steps of the preparation surface RC beams to increase the adherence of BFRP by epoxy.

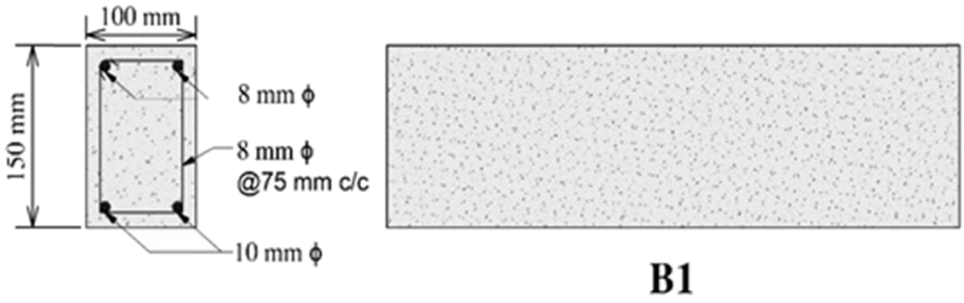

Figure 9: The control beam B1.

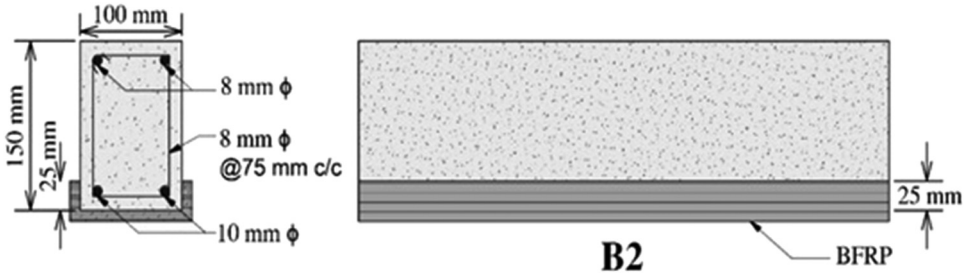

Figure 10: Beam B2 specifics of covering with BFRP sheets.

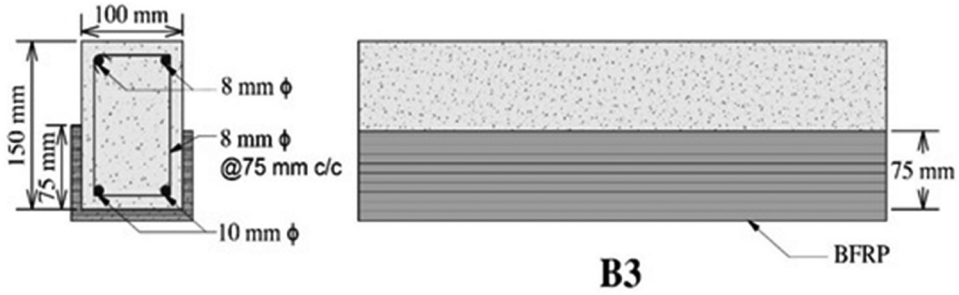

Figure 11: Beam B3 covers the BFRP sheets.

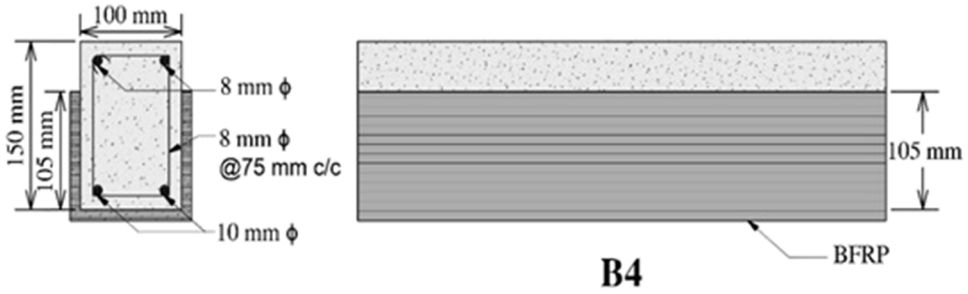

Figure 12: Beam B4 details of covering with BFRP sheets.

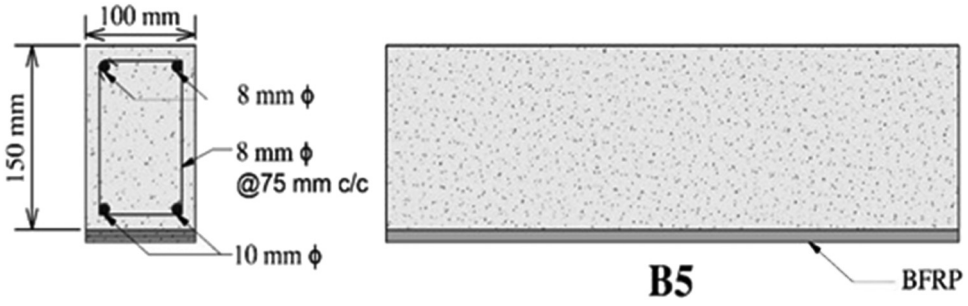

Figure 13: Beam B5 covers with BFRP sheets.

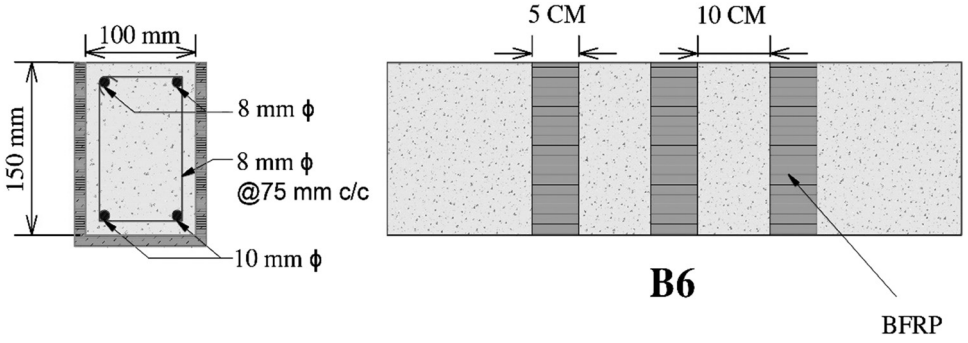

Figure 14: Beam B6 covers BFRP sheets.

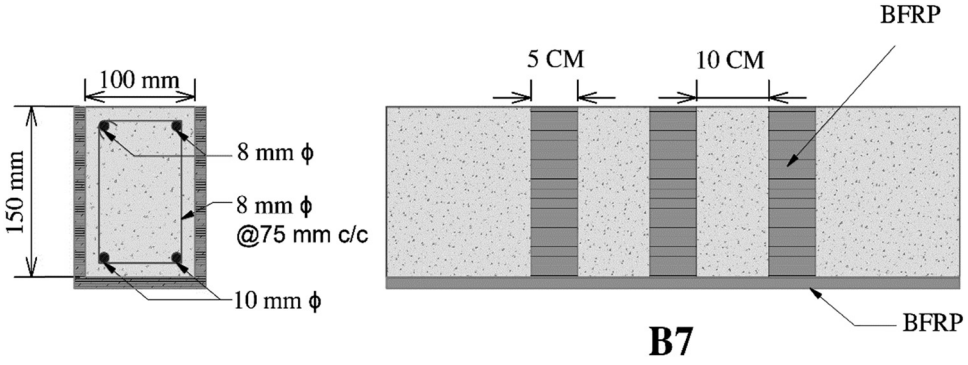

Figure 15: Beam B7 covers with BFRP sheets.

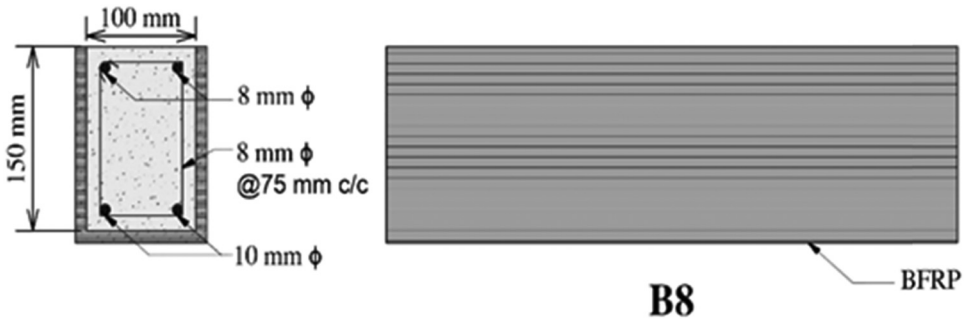

Figure 16: Beam B8 covers with BFRP sheets.

closed-loop servo-hydraulic testing system digital controller (Figure 17).

Finally, the beam was removed from the test equipment, and the concrete surface was examined at various angles; these tests were performed at Gaziantep University's College of Engineering in Gaziantep, Turkey.

8 Results and discussion of RC beams

The visuals of load vs mid-span deflection and the collapse shapes of all samples are included in the results. The reinforced beam's increased load-bearing capability, ductility, and crack pattern are investigated. Finally, the outcomes of the tests are reached and employed to compare the efficacy of BFRP laminates.

8.1 Relationships and failure modes of load–deflection

We studied the failure mode of each RC beam. Generally, the strengthened RC beam failure involved flexural cracks, crushing concrete, and BFRP rupture (Figure 18).

Beam (B1): To assess the behavior of the strengthened RC beams, the results of the unstrengthen control beam were used as a benchmark. The data were utilized to draw the load versus mid-span deflection curve, as shown in Figure 18. The ultimate load of 53.1 kN that corresponds to a deflection of 5.81 mm of the control beam is recorded. The failure deflection value was 15.82 mm. The beam failed in a typical flexural mode in which the reinforcement bars were deformed, followed by the crushing of the concrete on the upper surface of the beam in the middle section. The failure was mild, and there was adequate warning of impending failure,

Beam (B2): The RC beam strengthened was covered completely with BFRP sheets at the lower section and 25 mm height at both edges from the bottom in one layer has been tested to fail. From the test, as shown in Figure 18, the load versus mid-span deflection records were obtained. The obtained ultimate load was 72.82 kN, which corresponds to 13.76 mm vertical deflection. The recorded deflection value in the middle area of the failure was 13.94 mm. The percentage increase within the flexural capacity was 37%. The percentage decrease in ultimate and failure ductility values was 81 and 29%, respectively. The beam failed in a typical flexural mode in which the reinforcement bars were

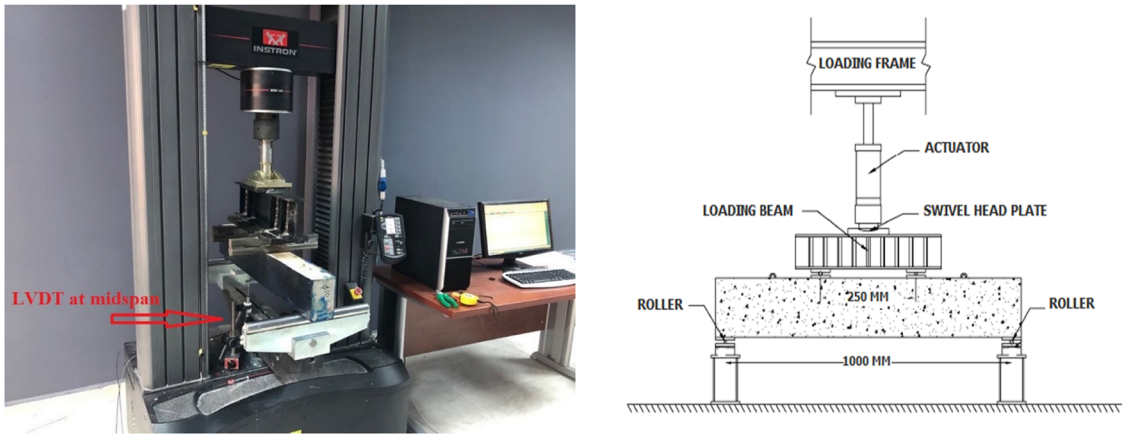

Figure 17: The flexure test setup.

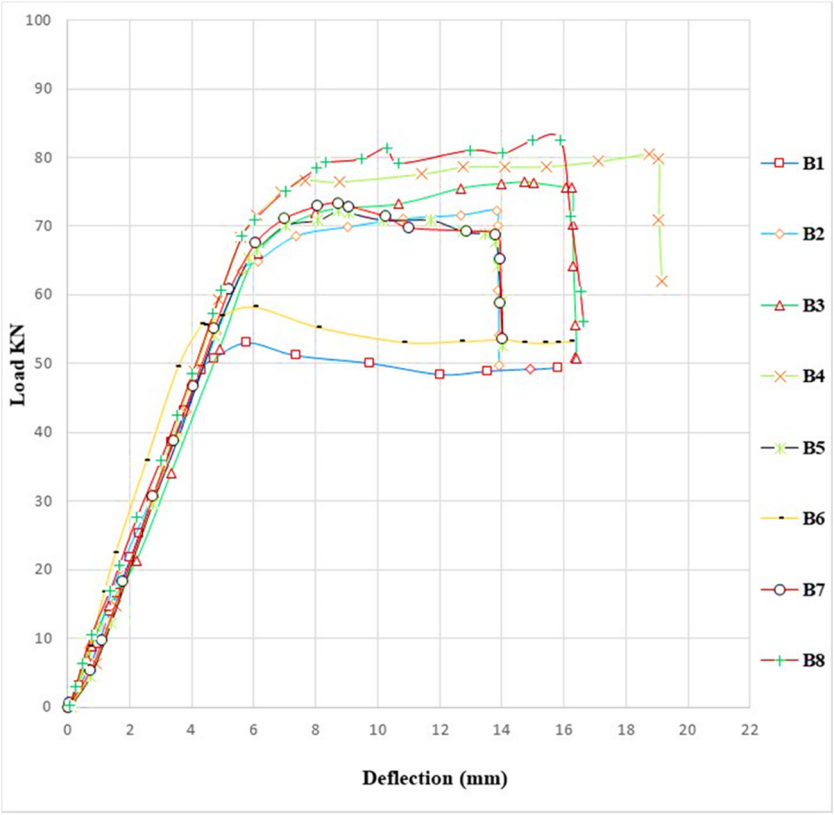

Figure 18: Load vs deflection for all beams.

deformed, followed by the crushing of the concrete on the upper surface of the beam in the middle section. The mode of failure was sudden, accompanied by the crushing of the compression concrete zone and a partial debonding of the BFRP.

Beam (B3): The RC beam strengthened was covered completely with BFRP sheets at the lower section and 75 mm height at both edges from the bottom in one layer has been tested to fail. The load versus mid-span deflection records were obtained from the test and presented in Figure 18. The obtained ultimate load was 76.55 kN that corresponds to a deviation of 14.58 mm. The deflection value in the middle area of the failure was 16.39 mm. The percentage increase within the flexural capacity was 44%. The percent reduction in ultimate and failure ductility values was 85 and 23%, respectively. The beam failed in a typical flexural mode in which the reinforcement bars were deformed, followed by the crushing of the concrete on the upper surface of the beam in the middle section. The mode of failure was sudden, with partial debonding of the BFRP sheet, which failed due to concrete crushing in the compression zone and some tearing-off of BFRP.

Beam (B4): The RC beam strengthened was covered completely with BFRP sheets at the lower section and 105 mm height at both edges from the bottom in one layer has been tested to fail. The load versus mid-span deflection records were obtained from the test, as shown in Figure 18. The obtained ultimate load was 80.55 kN that corresponds to a deflection of 18.53 mm. The deflection value in the middle area of the failure was 19.17 mm. The percentage increase within the flexural capacity was 52%. The percentage decrease in ultimate and failure ductility values was 89 and 28%, respectively. The beam failed by yielding the reinforcement rebar, tearing off the BFRP, and concrete crushing in the compression zone. The failure occurred with little obvious sign of impending collapse before the element failure.

Beam (B5): The RC beam strengthened was covered completely with BFRP sheets just at the lower section in one layer and was tested to fail. The load versus mid-span deflection records were found from the test, as shown in Figure 18. The obtained ultimate load was recorded to a value of 72.56 kN, which corresponds to a deflection of 9 mm. The deflection value of the mid-span at failure was recorded as a value of 14 mm. The percentage increase in the flexural capacity was recorded to a value of 36%. The percentage decline in the ultimate and failure ductility values was equal to 17 and 32%, respectively. The yielding of the reinforcement rebar caused the beam failure,

followed by BFRP debonding and failed due to concrete crushing in the compression zone, and the failure was relatively sudden and without warning.

Beam (B6): The strengthened RC beam was wrapped by BFRP fabrics as stirrups in the flexural zone portion in one layer was tested to fail. The load versus mid-span deflection records were gained from the test, as shown in Figure 18. The obtained ultimate load was recorded to a value of 58.28 kN, which corresponds to a deflection of 6.49 mm. The value of mid-span deflection at failure was recorded to a value of 16.20 mm. The percentage increase in the flexural capacity was recorded to a value of 9.4%. The percentage decline in the ultimate and failure ductility readings was equal to 5 and 0.2%, respectively. The yielding of the reinforcement rebar caused the beam failure, followed due to concrete crushing in the compression zone; the failure was not as mild as for the unstrengthen element but could not be described as "sudden."

Beam (B7): The strengthened RC beam was covered with BFRP fabrics just at the bottom with stirrups in the flexural zone portion in one wrap and was tested to fail. The load versus mid-span deflection records were gained from the test, as shown in Figure 18. The obtained ultimate load was recorded to a value of 73.56 kN, which corresponds to a deflection of 9.10 mm. The value of mid-span deflection at failure was recorded to a value of 14.25 mm. The percentage increase in the flexural capacity was recorded to a value of 38.53%. The percentage decline in the ultimate and failure ductility readings was equal to 19 and 33%, respectively. The yielding of the reinforcement rebar caused the beam failure, followed by BFRP debonding and concrete crushing in the compression zone. The failure happened suddenly and without warning.

Beam (B8): The RC beam enforced was wrapped at the bottom and two sides completely with one layer of BFRP fabric was tested to fail. The load versus mid-span deflection records were gained from the test, as shown in Figure 18. The ultimate load obtained was recorded to a value of 82.55 kN, which corresponds to a deflection of 15 mm. The value of mid-span deflection at failure was recorded as 16.64 mm. The percentage increase in the flexural capacity was equal to 56%. The percentage decrease in the ultimate and failure ductility readings was equal to 44 and 45%, respectively. The failure occurred suddenly, and there was no warning of impending failure from the deflections of cracking patterns. The destruction of BFRP and concrete crushing in the compression zone as.

When the fail modes of the various strengthened beams are compared in Table 4, it can be observed that the strengthened RC beams by one-wrap BFRP fabrics had the superior failure mode. The failure of these beams is due to BFRP wrap falling-out, indicating that the ultimate capacity of the BFRP wraps had been reached and the strengthening system was completely used [35].

Table 4: Brief of ultimate loadings and failure modes

Sample	P_{cr} (kN)	P_y (kN)	P_u (kN)	P_u/P_{uc}
Control B1	19	50.48	53.1	—
B2	29	64.74	72.82	1.37
B3	44	66.35	76.55	1.44
B4	63	72.70	80.55	1.51
B5	31	66.55	72.56	1.36
B6	35	55.59	58.28	1.09
B7	43	67.58	73.56	1.38
B8[b]	—	73.92	82.54	1.55

8.2 Ductility

The most widely used methods for calculating ductility from data are divided into two methods. The first one was the deflection ductility index ($\mu\Delta$), which is represented in equation (1) [32]

$$\mu\Delta = \frac{\Delta u}{\Delta y}. \quad (1)$$

A similar behavior was also observed. Attari et al. [33] also noticed that all of the strengthened specimens showed lower ductility than the control specimens.

The second method of estimating ductility was the energy ductility index (μ_E) by using equation (2) [32]

$$\mu_E = \frac{E_u}{E_y}. \quad (2)$$

Tables 5 and 6 summarize the measured ductility indications for total tested specimens.

Table 5 shows that beam B6 had a maximum ductility of 5%, while beam B4 had a minimum ductility of 89% in RC beam ductility compared with the un-strengthened beam. Generally, the ductility decreased with increasing amounts of strengthening.

Table 6 shows that the failure deflection index at beam B6 had a maximum of 0.5%, while the minimum failure index at beam B8 was 45% compared with the un-strengthened beam.

8.3 Crack patterns

As can be seen from the results presented, crack propagation in strengthened elements differs significantly from

Table 5: Brief of the deflection and ductility results

Sample	Deflection at yield (mm)	Deflection at ultimate (mm)	Deflection at failure (mm)	Ductility index		
				$\mu\Delta$	Increase %	μ_E
Control B1	4.71	6.01	15.79	1.27	—	1.4
B2	5.75	13.25	13.85	2.30	81	3.5
B3	6.27	14.84	16.27	2.36	85	3.3
B4	7.50	18.09	19.05	2.41	89	4.4
B5	6.11	9.12	13.91	1.49	17	1.69
B6	4.81	6.49	16.20	1.34	5	1.5
B7	6.19	9.45	14.03	1.52	19	1.75
B8	8.69	16.02	16.25	1.84	49	4.01

Table 6: Summary of the failure deflection index (I_f)

Specimen	$I_f = \Delta f/\Delta y$	I_f/I_{fc}[a]	Decrease %
Control B1	3.35	1	—
B2	2.44	0.71	29
B3	2.59	0.77	23
B4	2.54	0.75	25
B5	2.27	0.67	33
B6	3.36	1	0.5
B7	2.26	0.67	33
B8	1.86	0.55	45

[a]I_{fc} is the failure index of the control beam.

that of normally reinforced elements. This is to be expected as strengthened elements can be considerably stiffer than their non-strengthened counterparts, which understandably affects their behavior under loading.

Beam B1 control specimen has been loaded in a four-point bend test setup as described previously. The beams have been loaded with equal force on the two load points until the beams are deformed. The damage in the beams started with bending cracks in the central region of the beam, as shown in Figure 19. The first crack was observed at 19 kN. As load reached 52 kN, more cracks were observed. Almost all cracks were vertical. Near top and bottom edge sub-cracks were generated connecting to the main crack. The first crack generated was between the left point load and the beam center. The second crack was just inside the right point load. The third and fourth cracks generated were between the center point of the beam and the right point load. The fifth crack was just outside of the right point load. The sixth crack was between the third and fourth cracks. Major cracking was observed at 53.1 kN, and the beam stopped taking load after this point.

Beam B2, when load was applied on the beam, the first crack was observed at 29 kN. Spalling started at 52 kN load. The crackling sound of laminates was observed at 29 and 57 kN. Again, spalling was observed at 67 kN, as shown in Figure 20. Laminate failed at 72.82 kN by interfacial debonding. Loading was stopped after laminate failure.

Beam B3, when loading was started new crack was observed at 44 kN. The crackling sound was there at 69,

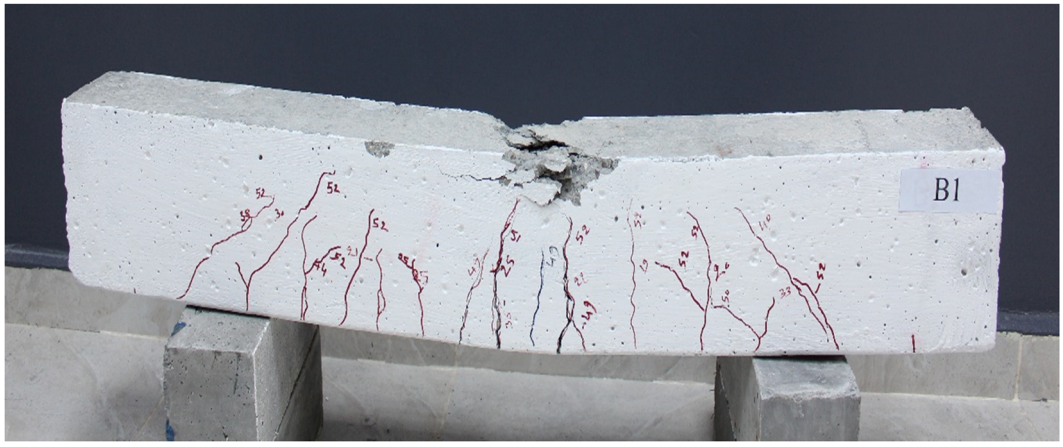

Figure 19: Crack pattern for beam B1.

Figure 20: Crack pattern for beam B2.

71, and 72 kN. Spalling started at 75 kN. Also, crackling sound was there in fibers at 75 kN as well. BFRP failed at 76.55 kN load, making the sound like a blast. Partial peeling off and partial debonding failure were observed, as shown in Figure 21.

Beam B4, when the load was applied on the beam, the first crackling was shown at 63 kN, and after that, again at 69, 71, and 76 kN, sound of the BFRP sheet was heard. Concrete crushing in compression at the top, as shown in Figure 22. The beam stopped taking further load at 80.55 kN. As compared to laminates, sheets did not fail over large area; only debonding was there in the bottom center. Debonding was not throughout the width of the beam.

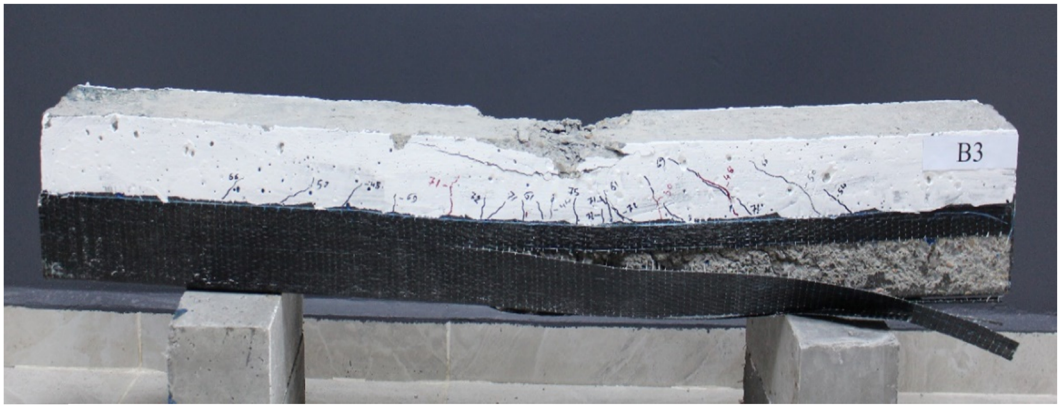

Figure 21: Crack pattern for beam B3.

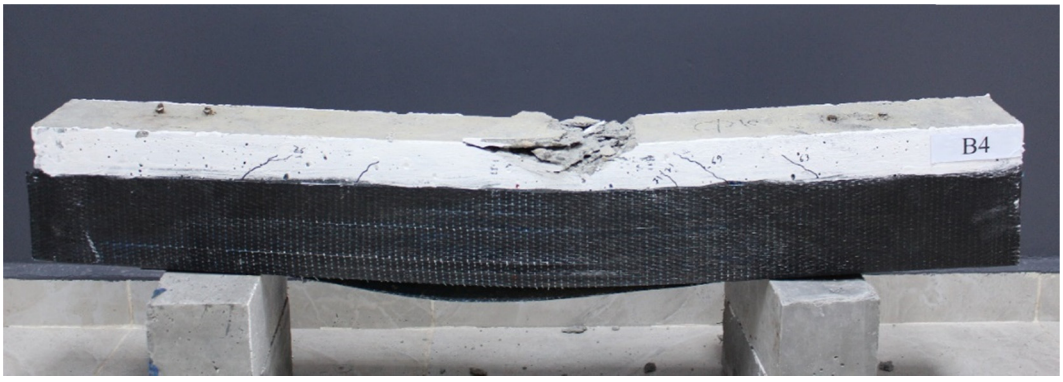

Figure 22: Crack pattern for beam B4.

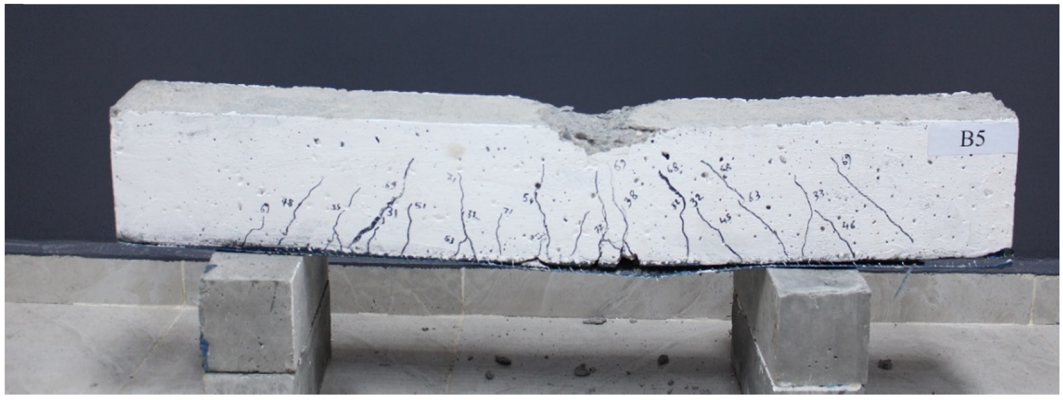

Figure 23: Crack pattern for beam B5.

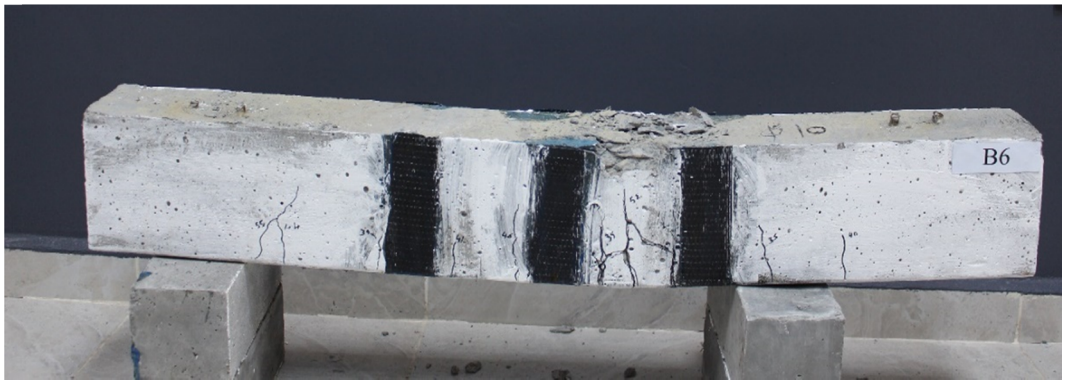

Figure 24: Crack pattern for beam B6.

An increase in load-carrying capacity was observed as the beam with BFRP failed at 80.55 kN.

Beam B5, the first crack, was observed at 31 kN. As load reached 58 kN, more cracks were observed. Almost all cracks were vertical; near the top and bottom edge sub-cracks were generated connecting to the main crack. Major cracking was observed at 69 kN. The beam stopped taking load at 72.56 kN. Partial debonding failure was observed in the tension zone, as shown in Figure 23.

Beam B6 shows similar behavior as beam B1. Therefore, steel was yielded in the specimen. The damage in the beams started with bending cracks in the central region of the beam, as shown in Figure 24; first crack was observed at 35 kN. As load reached 55 kN, more cracks were observed. Almost all

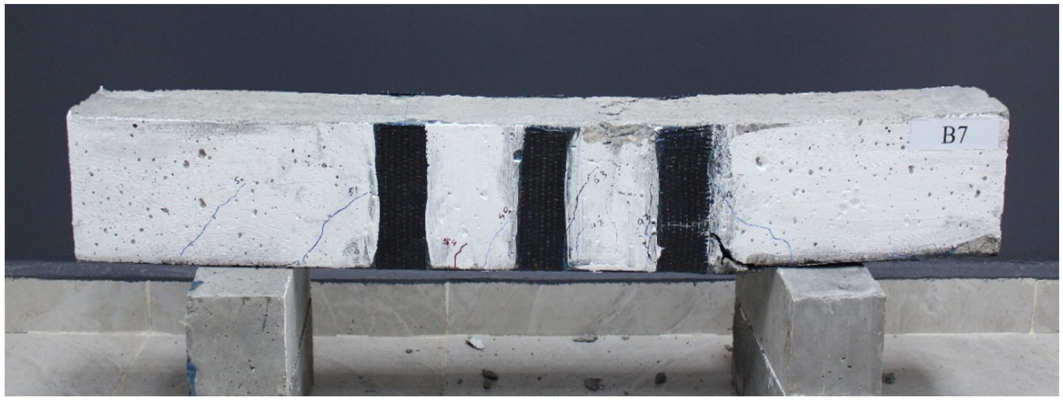

Figure 25: Crack pattern for beam B7.

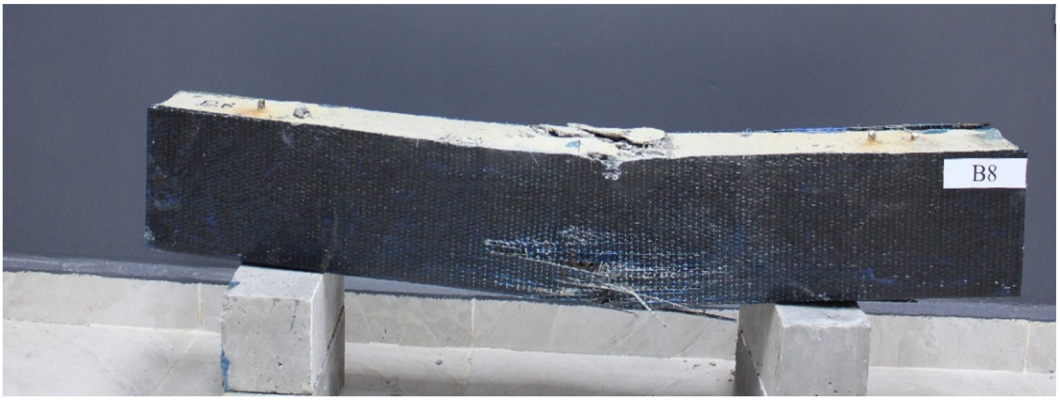

Figure 26: Crack pattern for beam B8.

cracks were vertical, and near the top and bottom edge sub-cracks were generated connecting to the main crack. The beam stopped taking load at 58.28 kN.

Beam B7, the first crack, was observed at 43 kN. As load reached 54 kN, more cracks were observed. Almost all cracks were vertical, and near the top and bottom edge sub-cracks were generated connecting to the main crack. Major cracking was observed at 63 kN. The beam stopped taking load at 73.56 kN, as shown in Figure 25.

Beam B8, U shape wrapped therefore no cracks could not be observed. The crackling sound was heard when loading was applied. The beam failed by flexural failure, rupture of BFRP, and crushing of concrete at the loaded point as shown in Figure 26. The beam stopped taking further load at 88.55 kN. The failure sound heard like a blast.

As can be seen from the results presented, crack propagation in strengthened elements differs significantly from that of normally reinforced elements. This is to be expected as strengthened elements can be considerably stiffer than their non-strengthened counterparts, which understandably affects their behavior under loading. The reason for this is that the presence of the basalt fiber composites helps to better distribute the tensile forces at the soffit of the element, which results in a reduction of the width and length of cracks that would normally be expected in an un-strengthened element. Due to debonding total utilization of the strength of the BFRP sheet was not achieved.

9 Conclusions

BFRP is considered a green material and has been illustrated to be a proper material for developing the infrastructure sustainability of RC members. This study has pointed out the need to enhance the knowledge of RC beams after strengthening by basalt fiber fabric. From the experimental test results presented, the following general conclusions can be drawn:

- The flexural capacity of the wrapped RC beams increases in percentage varied from 9.4 to 56% over the unwrapped beam.
- By comparing between the strengthened beams and unstrengthened beams, the percentage decline in the ductility varies from 5 to 89%.
- RC beams wrapped with a sheet of BFRP fabrics failed by FRP failure, taking into consideration that this FRP strengthening approach was completely used to its highest capacity.
- Excessive deformation occurs, and failure of the BFRP composites takes place. It should be noted that not all fibers may reach the ultimate limit state at the same time, which can result in a more gradual release of the stored elastic energy. This took place during the failure of beam B8, where distinct sounds of fibers snapping were noted before ultimate failure was reached.
- The adhesive bond between the fiber and the concrete substrate fails, resulting in a peeling off of the fiber composite sheet or plate along part or all of its length. This normally initiates at the end of the sheet or plate but, in some cases, can start elsewhere and propagate in two directions until failure occurs. Additionally, it is often the case that a delamination failure, as it propagates along the length of the beam, will become a tearing-off type failure. This occurs when the delaminating fiber composite sheet encounters a crack that is severe enough to allow the concrete cover to be torn away from the soffit of the beam, while remaining attached to the sheet. An example of this type of failure can be seen in B2, B3, B4, and B5.
- When an element is over-reinforced and/or over-strengthened in tension, the development of high compressive stresses in the compressive concrete zone results in a

sudden, sometimes "crushing," compressive failure of the concrete. In fact, the internal steel reinforcement has not normally even reached its yield point. An example of this type of crushing failure can be seen in all specimens.

- Crack propagation of crack widths for elements with externally bonded basalt fiber composites was investigated. It had already been shown that the occurrence of surface cracking in strengthened elements varied considerably from that of their unstrengthen counterparts. The main differences for strengthened elements can be summarized as follows and are attributable to the ability of the BFRP composites to better distribute the stress in the element soffit, resulting in a more consistent crack distribution: There is a higher number of surface cracks. Both the maximum and average crack lengths are shorter.

Acknowledgements: We acknowledge Dr. Minen Al-Kafajy for English observation and valued comments.

Conflict of interest: Authors state no conflict of interest.

Data availability statement: Data available within the article or its supplementary materials. The authors confirm that the data supporting the findings of this study are available within the article [and/or] its supplementary materials.

References

[1] Khanfour MA, El Refai A. Effect of freeze-thaw cycles on concrete reinforced with basalt-fiber reinforced polymers (BFRP) bars. Constr Build Mater. 2017;145:135–46.
[2] Zhou D, Lei Z, Wang J. In-plane behavior of seismically damaged masonry walls repaired with external BFRP. Compos Struct. 2013;102:9–19.
[3] Mostofinejad D, Kashani AT. Experimental study on effect of EBR and EBROG methods on debonding of FRP sheets used for shear strengthening of RC beams. Compos B Eng. 2013;45(1):1704–13.
[4] Yeboah D, Taylor S, McPolin D, Gilfillan R. Pull-out behaviour of axially loaded Basalt Fibre Reinforced Polymer (BFRP) rods bonded perpendicular to the grain of glulam elements. Constr Build Mater. 2013;38:962–9.
[5] Mostofinejad D, Mofrad MH, Hosseini A, Mofrad HH. Investigating the effects of concrete compressive strength, CFRP thickness and groove depth on CFRP-concrete bond strength of EBROG joints. Constr Build Mater. 2018;189:323–37.
[6] Wu G, Wang HT, Wu ZS, Liu HY, Ren Y. Experimental study on the fatigue behavior of steel beams strengthened with different fiber-reinforced composite plates. J Compos Constr. 2012;16(2):127–37.
[7] Ma G, Huang Y, Aslani F, Kim T. Tensile and bonding behaviours of hybridized BFRP-steel bars as concrete reinforcement. Constr Build Mater. 2019;201:62–71.
[8] Shi J, Wang X, Ding L, Wu Z. Degradation of creep behaviors of basalt fiber-reinforced polymer tendons in salt solution. J Mater Civ Eng. 2018;30:04018317.
[9] Chen ZF, Lee S, Ng M, Tang JM, Wan LL, Liu M, et al. Study of design configurations for strengthening RC slabs using BFRP. Sci Eng Compos Mater. 2008;15(3):165–74.
[10] Duic J, Kenno S, Das S. Flexural rehabilitation and strengthening of concrete beams with BFRP composite. J Compos Constr. 2018;22(4):04018016.
[11] Sim J, Park C, Moon DY. Characteristics of basalt fiber as a strengthening material for concrete structures. Compos Part B. 2003;36(6–7):504–12.
[12] Lihua H, Yujing L, Yuefang W. Strengthening effects of BFRP on reinforced concrete beams. J Southeast Univ. 2013;29(2):182–6.
[13] Fiore V, Scalici T, Di Bella G, Valenza A. A review on basalt fibre and its composites. Compos Part B: Eng. 2015;74:74–94.
[14] Pawłowski D, Szumigała M. An experimental and theoretical study of deflections of BFRP RC beams. Tech Trans Civ Eng. 2015;63–70.
[15] Shen D, Deng S, Zhang J, Wang W, Jiang G. Behavior of reinforced concrete box beam with initial cracks repaired with basalt fiber-reinforced polymer sheet. J Reinf Plast Compos. 2015;34(18):1540–54.
[16] Qin Z, Tian Y, Li G, Liu L. Experimental study on flexural capacity of severely pre-cracked RC beams reinforced with BFRP. J Build Struct. 2018;39(6):32–40 (in Chinese).
[17] Azeez AA, Jaafar AA, Yussof MM, Blash AA. Study of the behavior of reactive powder concrete RC deep beams by strengthening shear using near-surface mounted CFRP bars. Open Eng. 2023;13(1):20220433. doi: 10.1515/eng-2022-0433.
[18] AL-Asadi AK, Muttashar M, Almutairi AL. Modelling reinforced concrete beams for structural strengthening of buildings. Period Eng Nat Sci. 2020;8(2):1083–95.
[19] Ma G, Li H, Yan L, Huang L. Testing and analysis of basalt FRP-confined damaged concrete cylinders under axial compression loading. Constr Build Mater. 2018;169:762–74.
[20] Kadhim AM, Numan HA, Özakça M. Flexural strengthening and rehabilitation of reinforced concrete beam using BFRP composites: finite element approach. Adv Civ Eng. 2019;2019:4981750.
[21] Zhou YY, Yu JT, Lu ZD. Seismic behavior of BFRPreinforced pre-damaged concrete beam-column joints. J Cent South Univ Sci Technol. 2010;41:1514–21.
[22] Zhou YY, Lu ZD, Zhang KC. Experimental study on seismic behavior of strengthened RC column-beam joints damaged by simulated earthquake. J Build Struct. 2010;31:64–73.
[23] Yu JT, Su L, Lu ZD. Experimental study on BFRP damaged concrete beam-column joints by simulated earthquake. J Tongji Univ (Nat Sci). 2011;39:18–24.
[24] Wu G, Wei Y, Wu ZS. Comparative study on seismic performance of rectangular concrete columns strengthened with BFRP and CFRP composites. Ind Constr. 2007;37:14–8.
[25] 197-1, T.E. Cement- Part 1: Composition, specifications and conformity criteria for common cements, Turkish Standards; 2012.
[26] ASTM C618. Standard Specification for Coal Fly Ash and Raw or Calcined Natural Pozzolan for Use in Concrete. West Conshohocken, PA: ASTM International; 2012.
[27] http://www.basfcc.com.sg/en/products/ConcreteRepairandProtectionSystems/MBrace/MBraceSaturant/Pages/default.aspx.
[28] EFNARC. The European Guidelines for Self-Compacting Concrete, Specification, production and Use. Europe: EFNARC; 2005.

[29] Hollaway LC, Teng J-G. Strengthening and rehabilitation of civil infrastructures using fibre-reinforced polymer (FRP) composites. Elsevier; 2008.
[30] ACI 440. Guide for the design and construction of externally bonded FRP systems for strengthening concrete structures. Farmington Hills, MI, USA; 2008.
[31] ASTM C39. Standard test method for compressive strength of cylindrical concrete specimens. Annual book of ASTM standards. Vol. 4; 1997. p. 20–2.
[32] Spadea G, Bencardino F, Swamy RN. Structural behavior of composite RC beams with externally bonded CFRP. J Compos Constr. 1998;2(3):132–7.
[33] Attari N, Amziane S, Chemrouk M. Flexural strengthening of concrete beams using CFRP, GFRP and hybrid FRP sheets. Constr Build Mater. 2012;37:746–57.
[34] Dawood MH, Al-Asadi AK. Mechanical properties and flexural behaviour of reinforced concrete beams containing recycled concrete aggregate. Sci Rev Eng Environ Stud (SREES). 2022;31(4):259–69.
[35] Jaafar AA, Yussof MM, Azeez AA, Mezher TM, Ali Blash AA. The nonlinear analysis of reactive powder concrete effectiveness in shear for reinforced concrete deep beams. Open Eng. 2023;13(1):20220412. doi: 10.1515/eng-2022-0412.